

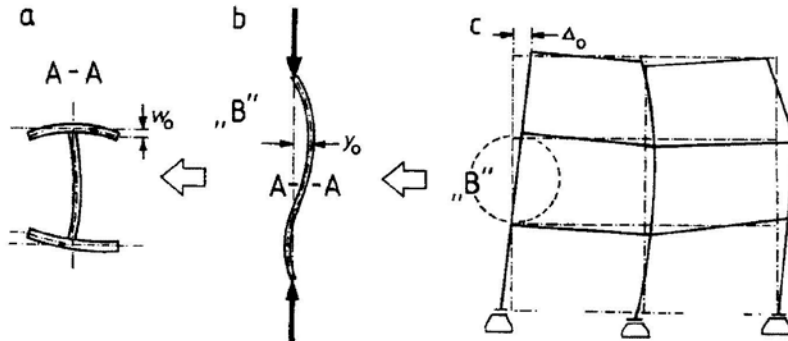
# Imperfections of axes and middle planes of elements

Antoni Biegus *Probabilistyczna analiza konstrukcji*

(*Probabilistic analysis of structures*) PWN 1999

The following **geometric imperfections of steel bar structures** occur:

- initial cross-sectional distortions—  $w_0$
- initial deflections of axes of bar elements—  $y_0$ ,
- deflected principal axes of a load-carrying system—  $\Delta_0$ .



Rys. 4.11. Imperfekcje geometryczne przekroju (a), pręta (b), systemu konstrukcyjnego (c)

Two-dimensional structures exhibit geometric imperfections of middle surfaces of shell elements and deflections of axes of structural systems.

Random imperfections of a cross-sectional shape  $w_0$  act on the random parameters of a cross section:  $A$ ,  $J_x$ ,  $J_y$ ,  $J_w$ .

**Imperfections** of axes of bar elements and middle surfaces of shell structures **decrease their limit load-carrying capacity.**

The random geometric imperfections lead to the variation of nodal coordinates:  $x_i$ ,  $y_i$ ,  $z_i$  and to the rotation  $\varphi_i$  of structural nodes.

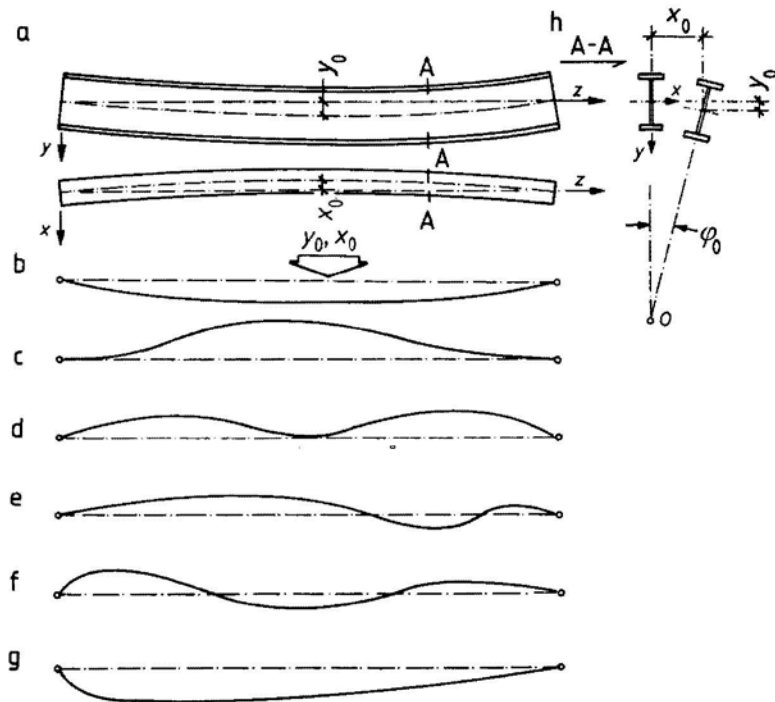
**The consequence of imperfections is a cross-sectional force variation with respect to the assumed perfect model.**

Statistically analysed geometric imperfections make up a basis for a **standard calibration of a group of factors**, e.g. of global and local instability, lateral torsional buckling.

**Geometric imperfections**, related to ideal geometry, may come from different sources:

- **random cross-sectional geometry** of a bar element – effect of hot-rolling or cold-forming of thin-walled members,
- **thermal processes imposed on members** (while welding in order to form a substructure) **and mechanical** processes at a production plant,
- transport and assembly actions at a building site.

Fig. 4.12a-g shows examples of initial **deflection of axes** of structural bar elements.

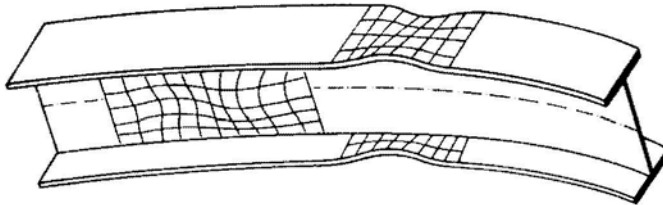


Rys. 4.12. Wstępne imperfekcje osi podłużnych prętów

The solid line in Figs. 4.12 a-g refer to bending related either to strong or to weak axis of inertia of the cross-section.

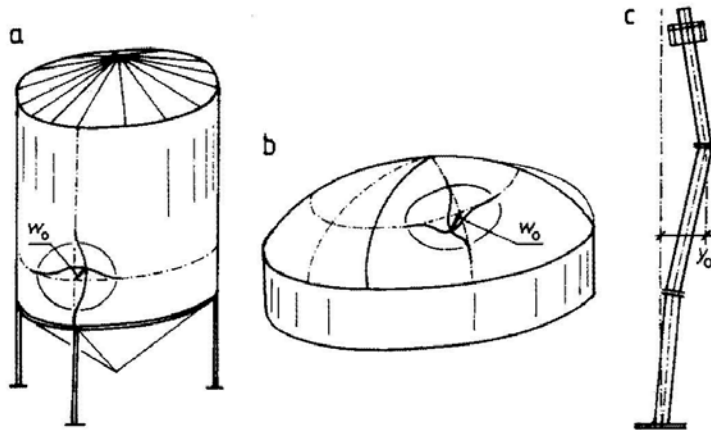
**Local geometric imperfection** may also occur – e.g. bulging or distortion of plate components of a section (web, flange).

Fig. 4.13 shows both global imperfection (deflection of the element axis) and local imperfections (initial distortion of flanges and initial bulging of web).



Rys. 4.13. Wstępne imperfekcje płaszczyzn środkowych elementów składowych prętów

Steel two-dimensional structures are subjected to local geometric imperfections, usually in the form of initial deflections (convexities and concavities) of a theoretical middle surface.



Rys. 4.14. Wstępne imperfekcje płaszczyzn środkowych silosu (a) i powłoki (b) oraz osi komina (a)

**Random imperfections are crucial for the limit load assessment of compressed structural members – bar elements or their parts – webs and flanges, also plates and shells, prone to buckling.**

The impact of axis or middle plane imperfections may be negligible only for elements at tension or at flexure with a sufficient bracing against local or lateral torsional buckling.

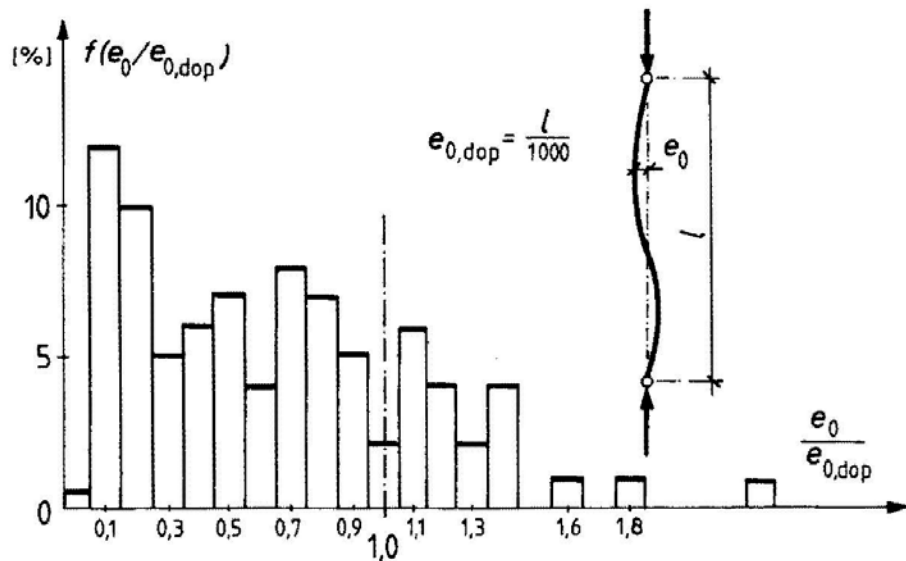
In each case of compression of imperfect structures (both at element and structure level) the following imperfections:  $x_0$ ,  $y_0$ ,  $\varphi_0$  and  $w_0$  produce both bending and compression.

**The limit load-carrying capacities of initially imperfect structures are less than their estimations for perfect structures.**

**The decisive imperfections for the limit load converge with the buckling modes (modes of stability loss) of elements or entire structures.**

The acceptance standards of civil engineering structures employ the initial structural imperfections by means of their limitation.

Fig. 4.15 shows the histogram of random deflections of elements, according to Sertler H., Vican J., Slavik J., *Compression Resistance of Steel Structure Members*, International Colloquium European Session "Stability of Steel Structures", Preliminary Report, vol. 1, s. 71-78, Budapest 1995.



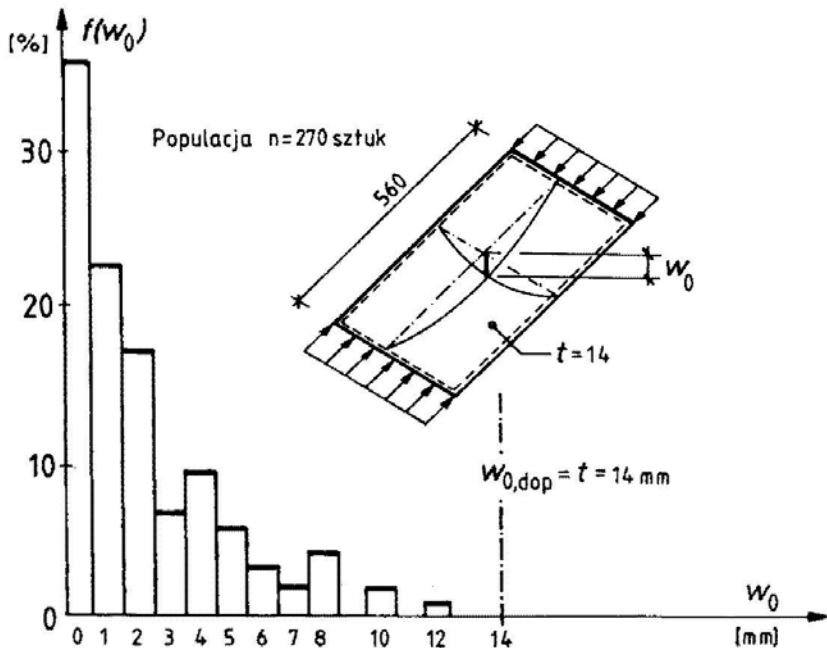
Rys. 4.15. Histogram wstępnych losowych odchyłek osi podłużnej prętów [73]

The abscissas in Fig. 4.15 show the measured values of  $e_0$ , scaled by the allowable standard value  $e_{0,dop}$ .

The majority of random realizations of initial deflections was less than the allowable value, but the histogram shows that excessive values exist in engineering structures.

The histogram of initial geometric imperfections of element axes may be considered a nonsymmetric distribution estimation.

Fig. 4.16 shows a histogram of initial random bulges (defects of the ideal middle plane) of 270 I-beam webs (plate elements)



Rys. 4.16. Histogram wstępnych losowych odchyłek płaszczyzny środkowej płyty [73]

All the investigated population exhibits initial imperfections of a middle plane not exceeding allowable values.

# Allowable geometric imperfections in standards

Probabilistic analysis of limit loads of structural elements does not employ geometric imperfections of axes of bars, assuming stochastic homogeneity (full autocorrelation of cross-sectional geometry) along the length of elements.

The initial deflections of axes of bars or concavities of plate and shell elements are significantly higher.

Transport of elements, their assembly into substructures are their possible causes.

The fabrication and acceptance standards of steel structures limit the initial imperfections related to the axis or a middle plane of an element, stating an upper boundary value or the distinct procedure in the case of exceedance.

The chosen geometric imperfections of tanks, according to a structural acceptance standard, are shown in Table 4.9

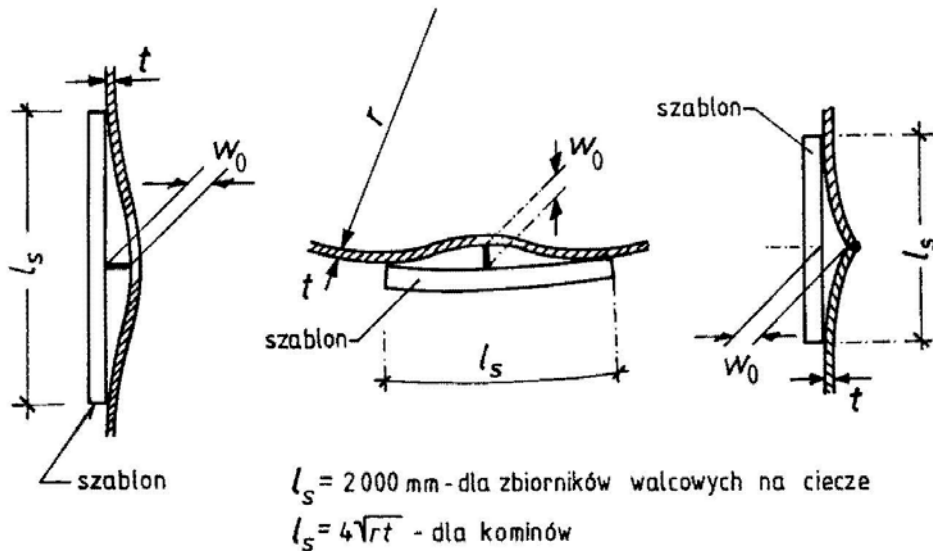
Tablica 4.9. Dopuszczalne odchyłki geometryczne płaszczy zbiorników wg [106]

| Poz.                             | Rodzaj odchyłki  |   | Średnica wewnętrzna zbiornika $d$ [m]      |                  |                  |                  |                |   |
|----------------------------------|--|---|--|------------------|------------------|------------------|----------------|---|
|                                  |  |   | $d \leq 10$                                | $10 < d \leq 20$ | $20 < d \leq 30$ | $30 < d \leq 50$ | $d > 50$       |   |
|                                  |  |   | Dopuszczalna odchyłka                      |                  |                  |                  |                |   |
| a                                | Odchyłka średnicy wewnętrznej płaszcza w odległości 300 mm od dna zbiornika <sup>1)</sup>                                      |   | $\pm 20$ mm                                | $\pm 25$ mm      | $\pm 40$ mm      | $\pm 45$ mm      | $\pm 60$ mm    |   |
| b                                | Odchyłka średnicy wewnętrznej płaszcza na poziomie górnej krawędzi ostatniego pasa <sup>1)</sup>                               |   | $\pm 25$ mm                                | $\pm 30$ mm      | $\pm 0,002 d$    | $\pm 0,002 d$    | $\pm 0,002 d$  |   |
| c                                | Różnica średnic dwóch sąsiednich pasów w tej samej płaszczyźnie pomiarowej <sup>1)</sup>                                       | zbiornik z dachem stałym                          | 20 mm                                      | 20 mm            | $0,0015 d$       | $0,0015 d$       | –              |   |
|                                  |  | zbiornik z dachem pływającym                      | 10 mm                                      | $0,0010 d$       | $0,0010 d$       | $0,0010 d$       | $0,0010 d$     |   |
| d                                | Różnica średnic płaszcza zbiornika na tej samej wysokości (w tej samej płaszczyźnie poziomej) <sup>1)</sup>                    | zbiornik z dachem stałym                          | 20 mm                                      | 20 mm            | $0,0015 d$       | $0,0015 d$       | –              |   |
|                                  |  | zbiornik z dachem pływającym                      | $0,0010d$                                  | $0,0010 d$       | $0,0010 d$       | $0,0010 d$       | $0,0010 d$     |   |
| e                                | Odchyłka wysokości płaszcza zbiornika <sup>1),2)</sup>   |   | $\pm 0,0020 h$                             |                  |                  |                  |                |   |
| f                                | Strzałka odchylenia tworzących płaszcza od pionu <sup>2)</sup>   |   | $\pm 0,0050 h$                             |                  |                  |                  | $\pm 0,0045 h$ |   |
| g                                | Lokalne odkształcenia (wypukłości i wklęsnięcia na powierzchni w obrębie jednego pasa)   | mierzone szalonym kołowym o długości 2 m          | strzałka ugięcia powierzchni odkształconej | 20 mm            |                  |                  |                |   |
|                                  |  |   | ilość powierzchni odkształconych           | 4                | 4                | 6                | 6              | 6 |
|                                  |  | mierzone pionowym szalonym linowym o długości 2 m | strzałka ugięcia powierzchni odkształconej | 20 mm            |                  |                  |                |   |
| ilość powierzchni odkształconych | 2  |   | 2  | 2                | 4                | 4                |                |   |
| h                                | Różnica obwodów płaszcza w dwu sąsiednich pasach mierzona w środku pasa (dotyczy zbiorników z dachem pływającym) <sup>2)</sup> |   | 0,001 obwodu                               |                  |                  |                  |                |   |

<sup>1)</sup> Pomiary wykonać co najmniej w czterech punktach pomiarowych równomiernie rozłożonych na obwodzie, maksymalna odległość punktów pomiarowych  $l_{max} = 6$  m.

<sup>2)</sup> Pomiary należy wykonać po próbie wodnej.

The inspection procedure(check) of geometric imperfections of shell steel structures (tanks, chimneys, pipelines) is shown in Fig. 4.21



Rys. 4.21. Sposób kontroli wad geometrycznych powłok walcowych

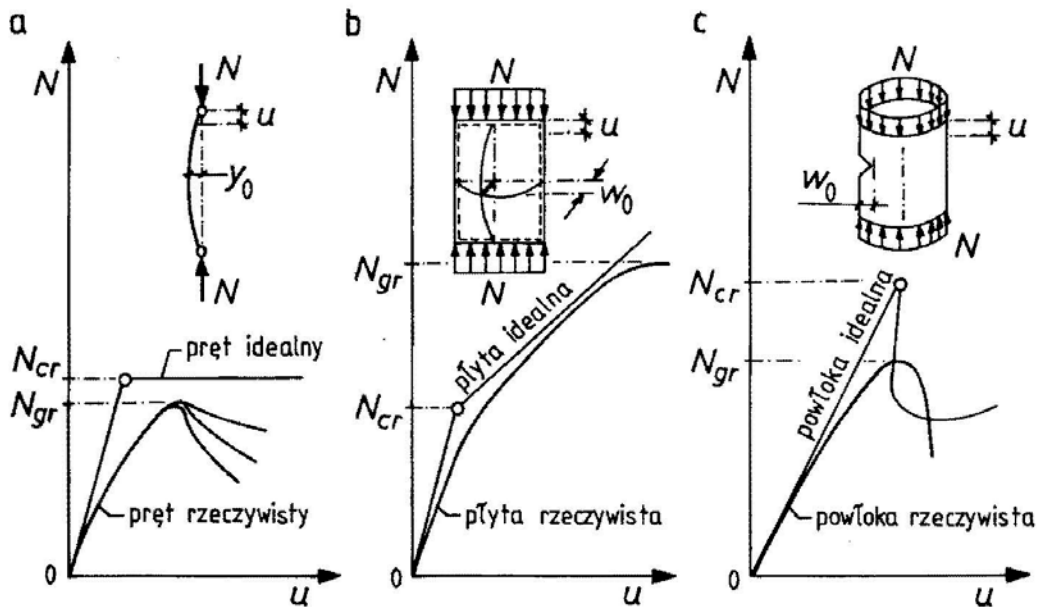
The standard allows for a number of vertical local distortions much less than a number of horizontal ones.

The standard rule presented above is easy to explain by means of static and strength criteria – the possibility of stability loss of a cylindrical shell.

# Impact of geometric imperfections on structural strength

The theoretical **static equilibrium paths** (load-contraction relations) of perfect, ideally compressed bars, plates and shells are shown in Fig. 4.22 by thin lines. Solid lines in the same figures depict the real, geometrically imperfect structures.

The static equilibrium paths (in Polish – ŚRS) of both perfect and real structures, shown in Fig. 4.22 diverge significantly, especially in the post-critical region (after the stability loss).



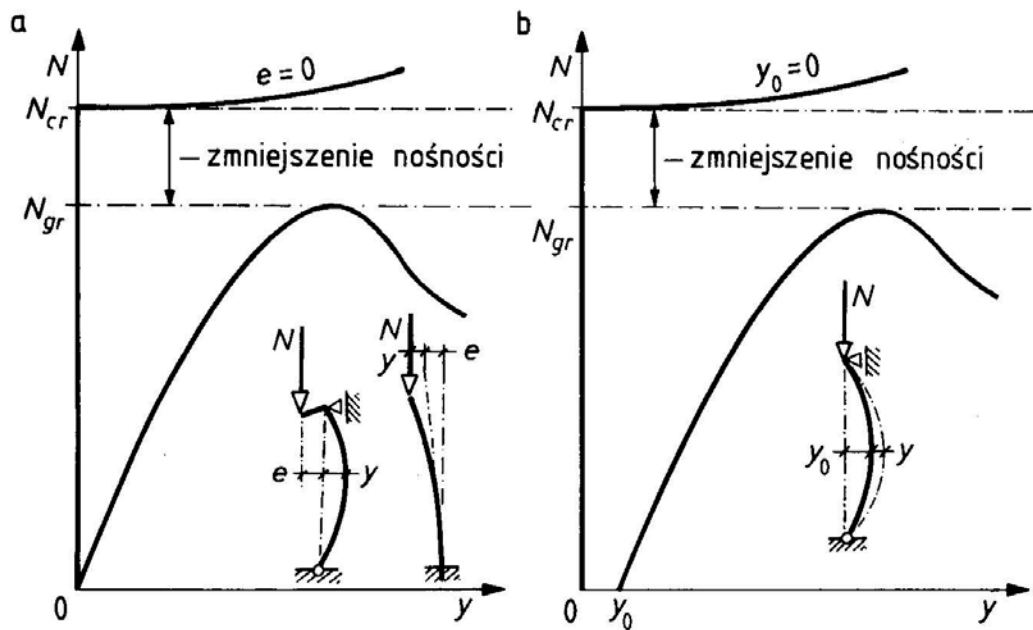
Rys. 4.22. Ścieżki równowagi statycznej: a – pręta, b – płyty, c – powłoki

The Euler's model of a bar at compression is not fully applicable. The **load-carrying capacity** of a real element,  $N_{lim}$  is less than its **theoretical critical force**,  $N_{cr}$ .

The main reason is the non-straight initial form of real compressive members (the so-called flexural factor).

The axes of real elements at compression may be imperfect, additionally, the load may be randomly eccentric.

The impact of deflected element axis and eccentric load on the load-carrying capacity is shown in Fig. 4.23.



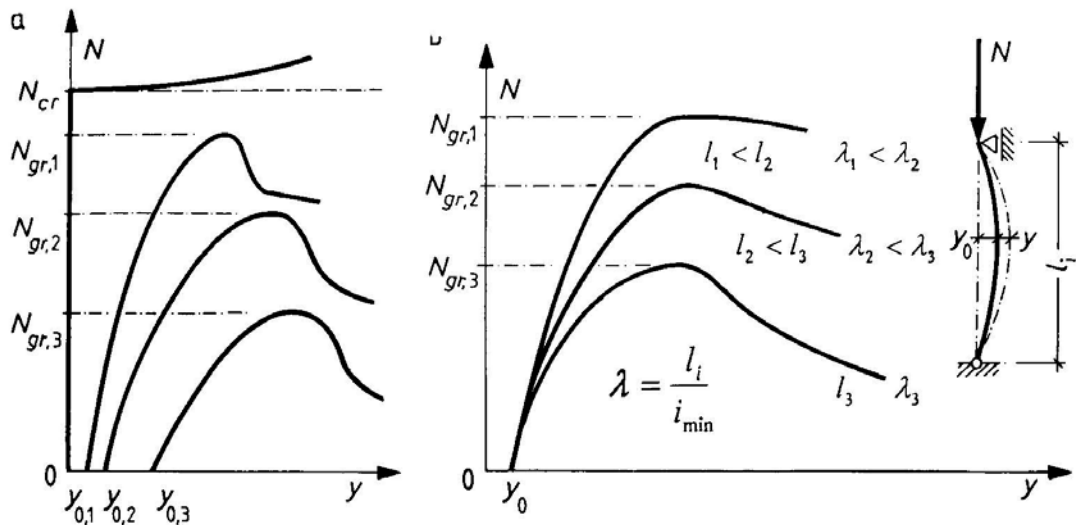
Rys. 4.23. ŚRS prętów ściskanych mimośrodowo (a) i ze wstępną krzywizną (b)

The static equilibrium paths in Fig. 4.23 are all curvilinear, similarly shaped.

The differences between  $N_{cr}$  and  $N_{lim}$  for compressive members increase nonlinearly with the element axis imperfections and eccentricity of the axial load.

Fig. 4.24 presents the decrement of limit load-carrying capacity of elements at compression.

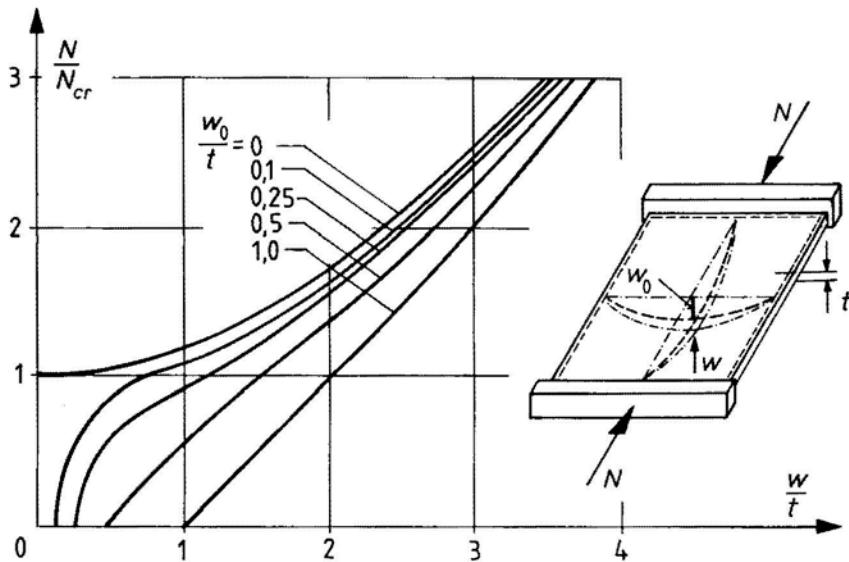
Slender elements are more sensitive to the impact of initial imperfections than the thick ones. The limit load decrement (from  $N_{cr}$  to  $N_{lim}$ ) for slender elements is shown in Fig. 4.24b.



Rys. 4.24. Ścieżki równowagi statycznej prętów ściskanych o różnych imperfekcjach geometrycznych (a) oraz o różnych smukłościach (b)

Analysis of static equilibrium path of a compressed bar makes us conclude that achieving the limit load  $N_{lim}$  means that the member is no longer load-resistant.

The equilibrium paths of plates at compression with initial geometric imperfections  $w_0$  are shown in Fig. 4.25



Rys. 4.25. Ścieżki równowagi granicznej płyt ściskanych z imperfekcjami geometrycznymi  $w_0$

The diagrams in Fig. 4.25 show that the plate imperfection value  $w_0$  does not affect its limit load  $N_{lim}$ , which may be several times higher than the critical load  $N_{cr}$ .

The Euler model of a perfect plate loaded in its middle plane allows to determine its compressive (shear) critical load  $N_{cr}$ , similarly to the one-dimensional cases.

Contrary to bar analysis, supercritical load (often called post-critical) of a plate is higher than its critical load.

Limit load in the subcritical (pre-critical) loading phase – equivalent to elastic allowable load – is a partial application only of a full limit load-carrying capacity of the element, the local stability loss (bulge of a plate at compression or shear) is not a structural failure mode.

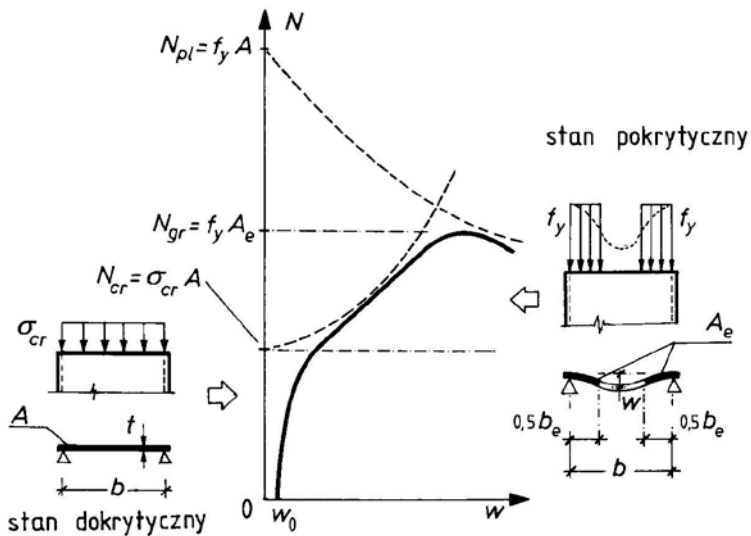
**Thus application is done of the fact that plates may carry significant loads in the supercritical region.**

The supercritical state is marked by a nonlinear stress distribution along the plate width. Limit state is reached by means of yielding of the supporting edges, parallel to load.

Such strength model of a plate incorporates the so-called effective width of compressive flanges, employed in the supercritical limit load theory.

It assumes that a quantitatively distinct supercritical equilibrium of a plate is possible, in the range of finite deflections.

The static equilibrium path of a real both-side supported plate at compression is shown in Fig. 4.26



Rys. 4.26. Ścieżka równowagi statycznej płyty

The unavoided geometric imperfections  $w_0$  make both equilibrium paths diverge: the first related to the real steel member (web, flange), the second – theoretical Euler's solution.

The critical load of a plate is not identical to its maximum load carrying capacity. The plate transfers to its supercritical phase, accompanying deflection increment is easily observed, stress redistribution in the cross-section occurs.

Load-carrying capacity loss at the limit state produces negative increment – resistance reduction at  $w > w_{lim}$ . It is the result of a nonlinear, flexural failure mode, corresponding to the altered equilibrium pattern.

A failure mode of a thin-walled element may be plastic buckling of a boundary supporting the compressive plate.

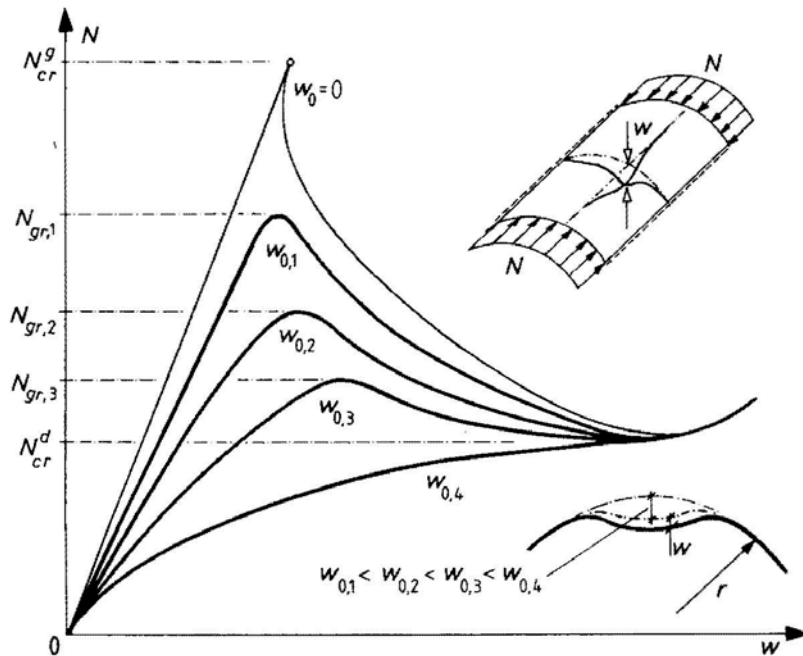
The conclusion of limit state analysis of plate strips at compression (thin-walled section elements), both sides supported (webs of I-sections, flanges and webs of box girders) is a significant safety reserve after the onset of local buckling.

Their limit load-carrying capacity is much higher than the critical load,  $N_{lim} > N_{cr}$ .

The initial geometric imperfections do not affect the limit load of plates,  $N_{lim}$ , as strongly as in the case of bars at compression.

The supercritical limit load of plates supported along the load direction (compressed plate elements of steel structures) is valid for the assessment of a limit load of thin-walled bar elements.

**The static equilibrium path of an ideal compressed shell** (thin line) and a real shell (solid lines) are shown in Fig. 4.27



Rys. 4.27. Ścieżki równowagi granicznej powłok z różnymi imperfekcjami geometrycznymi

Analytical assessment of critical limit load-carrying capacity due to linear theory is very erroneous (up to several times). Thus in

practice experimental results may be applied or the limit loads for imperfect shells may be investigated.

Imperfections amplify structural deflections and reduce the limit load to the so-called lower critical value  $N_{cr}^d$ .

Static equilibrium paths of real shells exhibiting random initial geometric imperfections (concavities) are shown in Fig. 4.27

The results show reduction of limit load of a shell with the geometric imperfection and deflection increment.

After reaching the limit load-carrying capacity of a shell its resistance is reduced.

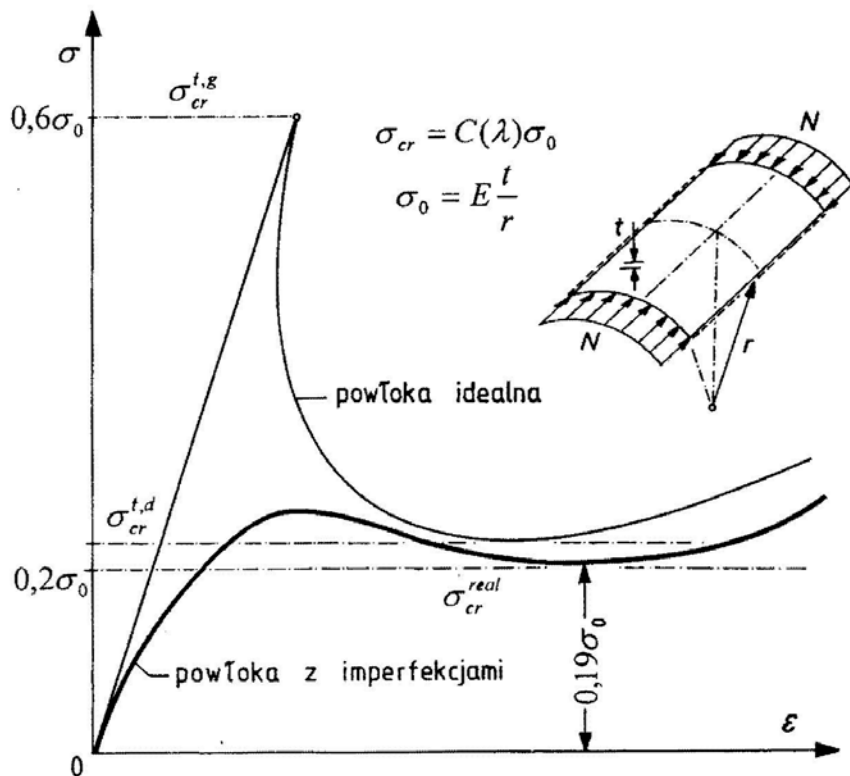
The real limit load of a shell,  $N_{lim}$ , is much smaller than the theoretical estimation of its critical load,  $N_{cr}^g > N_{lim}$

The static equilibrium paths of real, imperfect compressed shells and bars are qualitatively similar, but the impact of imperfections on the limit load is much greater for shells. This comes from different sources of physical and geometric nonlinearities and the initial imperfections of the theoretical shape of a shell (geometric imperfections of shells).

This computational model is valid for cylindrical and spherical tanks, chimneys, pipelines, cylindrical framed shells and framed domes.

Fig. 4.28 shows numerical differences between theoretical limit load of a perfect shell,  $\sigma_{cr}^{t,g}$  (upper estimation of theoretical value),  $\sigma_{cr}^{t,d}$  (lower estimation of theoretical value) and a real imperfect shell,  $\sigma_{cr}^{real}$ .

The analysis of limit loads of shells makes us predict that the resistances of real structures may be much smaller than their upper theoretical estimations.



Rys. 4.28. Teoretyczne i rzeczywiste nośności powłok walcowych

# Limit load estimation considering geometric imperfections

Theoretical and experimental research on metal civil engineering structures brought about the impact of structural, technological and geometric imperfections to the standards of design of bars, plates and shells, thus considering their real limit loads.

Calibrating the instability coefficients for steel compression members used in the standards incorporates technological and geometric imperfections in real structures (e.g. in the form of initial axial load eccentricities).

Limit loads estimation of an axially compressed bar element assumes sinusoidal shape of initial imperfection of its axis, the maximum deflection equal to

$$y_{02} = 0,002l \tag{1}$$

$$\text{or } y_{02} = 0,05i_{\min} + 0,002l \quad (2)$$

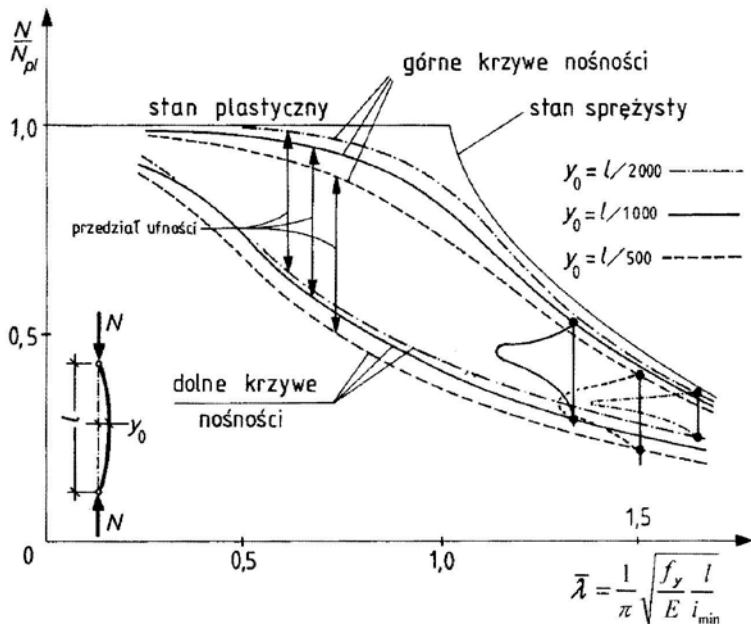
where

$l$  – length of a bar,

$i_{\min}$  – minimum radius of inertia of its cross-section

A database of identified random imperfections of the element axis or the plate middle plane allows for the probabilistic analysis of the limit state in the case of compression and bending interaction (second order theory due to bars, plates, shells), assuming the value of geometric defect of an axis or a middle plane.

This sort of analysis of compressed bars is illustrated in Fig. 4.29. The initial sinusoidal curvatures are determined by a maximum deflection  $y_0$  at the midspan, of the following values:  $l/500$ ,  $l/1000$  and  $l/2000$  ( $l$  – length of a compression member).



Rys. 4.29. Krzywe wyoboczeniowe ściskanych prętów z imperfekcjami geometrycznymi [27]

This figure shows upper and lower limit load curves for imperfect bar elements.

The increment of initial deflection  $y_0$  of a compression element axis reduces the mean limit load of considered elements and the lower limit load curve, reducing the confidence interval for a prescribed failure probability  $f$ .

Geometric imperfections of bar element axes may be described by nonsymmetric probability distributions. Geometry of axis – its random maximum deflection may be linked with the Gumbel (Extreme type I) distribution of a given probability density function

$$f(y_0) = \nu e^{-\nu(y_0-q)} - e^{\nu(y_0-q)} \quad (3)$$

The central value  $\bar{y}_0$  and characteristic deviations  $s_{y_0}$  of the random deflection are estimated as follows

$$\bar{y}_0 \approx g - \frac{0,577}{\nu} \quad (4)$$

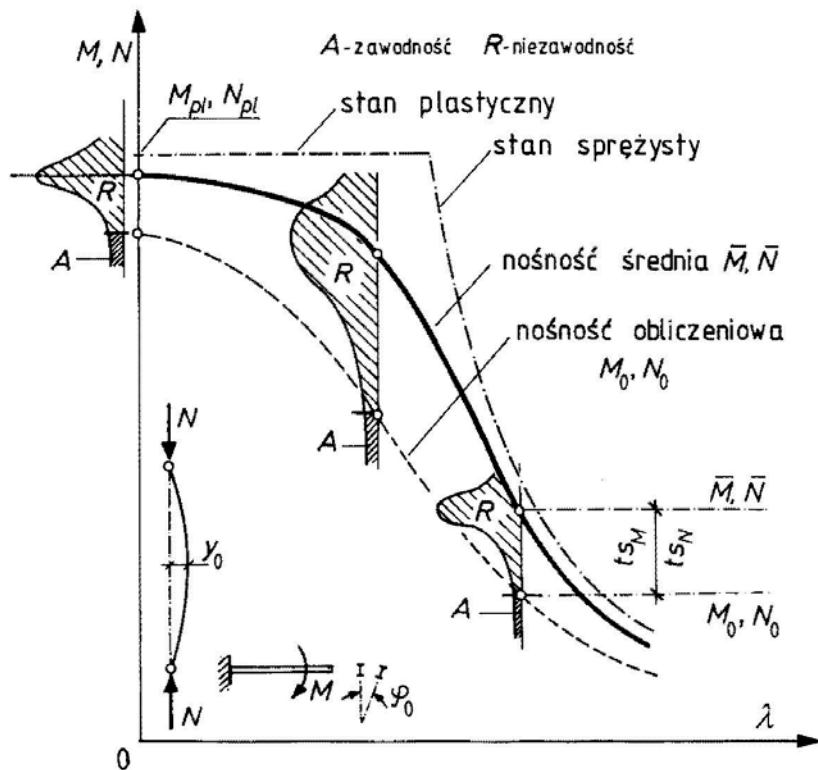
$$s_{y_0} \approx \frac{1,282}{\nu} \quad (5)$$

where

$q$  – the modal value (mode) of initial deflection,

$v$  – scatter measure of the initial deflection.

Fig. 4.30 shows the limit load estimation due to the global instability check of members at compression and bending (no lateral torsional bracing) of imperfect elements, by means of probabilistic methods.



Rys. 4.30. Wyznaczanie krzywych wyboczeniowych utraty stateczności ogólnej

Buckling curves in Fig. 4.30 define the limit load: axial  $N$  or flexural  $M$  on ordinates, slenderness  $\lambda$  on abscissas.

The solid line in Fig. 4.30 indicates a mean limit load curve, experimentally or theoretically derived for an assumed initial curvature of an axis given a deflection  $y_0$ .

The dashed line shows the design limit load elements at compression or bending of an assumed safety level.

The impact of geometric imperfection on a load-carrying capacity is crucial for compressed cylindrical shells (e.g. tanks, silos, chimneys) and spherical shells (e.g. tanks, domes). In these cases theoretical limit loads are several times greater than the limit loads of geometrically imperfect real structures.